Available online at www.sciencedirect.com
ScienceDirect
Journal of Power Sources 173 (2007) 556–561
JOURNAL OF POWER SOURCES
www.elsevier.com/locate/jpowsour

Short communication

Reaction mechanism and kinetics of lithium ion battery cathode material $LiNiO_2$ with CO_2

Hansan Liu [a], Yong Yang [b], Jiujun Zhang [a,*]

[a] *Institute for Fuel Cell Innovation, National Research Council of Canada, Vancouver, BC V6T 1W5, Canada*
[b] *State Key Laboratory for Physical Chemistry of Solid Surfaces, Xiamen University, Xiamen 361005, China*

Received 16 April 2007; received in revised form 30 April 2007; accepted 30 April 2007
Available online 6 May 2007

Abstract

The reaction between $LiNiO_2$ and CO_2 is relevant to the synthesis and storage of $LiNiO_2$-based cathode materials for lithium ion batteries. In this work, this reaction was investigated in pure CO_2 atmosphere at both room and high temperatures. The reaction products (Li_2CO_3, NiO, and O_2) and activation energies were determined by means of XRD, XPS, MS and TGA techniques. The reaction mechanism was explored in an effort to clarify some inconsistencies in the previous works. Kinetics analysis was also carried out to understand the reaction process relevant to the synthesis and storage of $LiNiO_2$ cathode material.

Keywords: Lithium nickel oxide; Carbon dioxide; Reaction mechanism; Kinetics analysis; Cathode material; Lithium ion batteries

1. Introduction

Lithium nickel oxide ($LiNiO_2$), which has an analogous layered structure to the commercially available lithium cobalt oxide ($LiCoO_2$), is a kind of promising cathode material for lithium ion batteries [1]. $LiNiO_2$ is superior to $LiCoO_2$ with respect to cost and specific capacity. However, the disadvantages of the $LiNiO_2$ material have been identified as low reproducibility, fast capacity fading, thermal instability, and poor storage property [2]. In order to overcome these technical barriers, tremendous effort has been made in developing lithium nickel oxide and its derivates as practical cathode materials [3–13].

One of the concerns is the presence of surface lithium carbonate (Li_2CO_3) on the $LiNiO_2$-based materials, which is formed through the reaction of lithium nickel oxides with CO_2 in air [5–7,10–15]. It has been recognized that lithium carbonate is electrochemically inactive due to its poor electronic conductivity and low lithium ion conductivity, impeding lithium ion intercalation or deintercalation reactions within the cathode [7]. Furthermore, lithium carbonate also easily reacts with electrolyte to result in gas evolution during battery operation, which could cause safety issues [7]. The formation of lithium carbonate during $LiNiO_2$ storage in air can also result in changes in surface or bulk structure and composition, which is the major cause of poor storage property of $LiNiO_2$-based materials [12]. Moreover, the reaction between $LiNiO_2$ and CO_2 also affects the reproducibility of $LiNiO_2$ synthesis through the most used precursors NiO and Li_2CO_3. Thus, a fundamental understanding of the mechanism and kinetics of the reaction between $LiNiO_2$ and CO_2 is necessary for the development of $LiNiO_2$-based cathode materials.

In the literature [5–7,10,11], the formation of Li_2CO_3 on the $Li_{1-x}NiO_2$ surface is believed to be through the following reaction:

$$LiNiO_2 + 0.5xCO_2 + 0.25xO_2 \rightarrow Li_{1-x}NiO_2 + 0.5xLi_2CO_3 \quad (1)$$

where the lithium ion would deintercalate from the mother material ($LiNiO_2$) to combine with CO_2, and O_2 would participate as a reactant to provide an extra oxygen source for the formation of Li_2CO_3. As a result of the redox reaction (1), a part of Ni^{3+} in the mother material would be oxidized to Ni^{4+}. However, our previous studies [12,13] on the storage property of $LiNiO_2$-based materials in air indicated that Ni^{2+} rather than Ni^{4+} was formed after $LiNiO_2$ reacted with atmospheric CO_2, with a contribu-

* Corresponding author. Tel.: +1 604 221 3087; fax: +1 604 221 3001.
E-mail address: jiujun.zhang@nrc.gc.ca (J. Zhang).

0378-7753/$ – see front matter.
doi:10.1016/j.jpowsour.2007.04.083

tion from active oxygen species in the bulk material. Recently, Shizuka et al. [15] confirmed our observation by the study of the effect of CO_2 on $Li_{1+z}MO_2$ ($M = Ni_{0.8}Co_{0.15}Al_{0.05}$), and proposed the following reaction:

$$LiMO_2 + 0.5xCO_2 \rightarrow 0.5xLi_2CO_3 + Li_{1-x}MO_{2-x} + 0.25xO_2 \quad (2)$$

where O_2 was thought to be decomposed from the mother material, although no evidence was provided.

Obviously, there exist some inconsistencies in the literature regarding the reaction mechanism between lithium nickel oxide and carbon dioxide. The main discrepancies are: (1) what is the nickel oxidation state after the reaction; (2) what is the extra oxygen source of the Li_2CO_3 formation. In order to clarify the mechanism, more evidence for the reaction products is necessary.

In this work, the reaction between $LiNiO_2$ and CO_2 was investigated in a pure CO_2 atmosphere at both room and high temperature. The reaction products were determined using X-ray diffraction (XRD), X-ray photoelectron spectroscopy (XPS) and mass spectroscopy (MS). The reaction activation energy was also calculated based on thermal gravitometer analysis (TGA) with discussion of the reaction kinetics relevant to the synthesis of $LiNiO_2$.

2. Experimental

Fresh $LiNiO_2$ was synthesized by a sol–gel method using citric acid as a chelating agent, as reported in our previous works [8,9]. Briefly, a citric acid solution with nickel nitrate and lithium hydroxide was stirred in an 80 °C water bath for 12 h to produce a gel. After drying in a vacuum at 120 °C for 24 h, the gel was then heat-treated in a Muffle oven at 500 °C for another 6 h. Then, the obtained black powder was sintered in a tube furnace at 725 °C for 24 h with oxygen flow at a rate of 800 ml min^{-1}. The metal composition of fresh material obtained was measured by inductively coupled plasma-mass spectrometry (ICP-MS, HP4500).

The reaction of $LiNiO_2$ with CO_2 at room temperature was carried out in a dry glass vessel where the $LiNiO_2$ powder was exposed to a constant CO_2 (99.999%) flow at a flow rate of 50 ml min^{-1} for 6 months. The reaction of $LiNiO_2$ with CO_2 at high temperature occurred in a tube furnace with a constant CO_2 (99.999%) flow at a flow rate of 300 ml min^{-1}. During the high temperature reaction, the $LiNiO_2$ sample was placed in a ceramic combustion boat. For the 650 °C reacted sample, the temperature was increased with a rate of 5 °C min^{-1} to 650 °C and stayed at this temperature for 10 min to complete the reaction with CO_2. For the 900 °C sample, the same heating rate was used and the sample also stayed at 900 °C for 10 min. Powder X-ray diffraction coupled with Rietveld refinement analysis (XRD), X-ray photoelectron spectroscopy (XPS), and mass spectroscopy (MS) were used to analyze the samples before and after reaction to determine the reaction products. XRD was operated on a Rigaku Rotaflex D/max-C diffractometer. The Rietveld refinement analysis was carried out in the software of general structure analysis system (GSAS) [16]. The structure model of $[Li_{1-x}Ni_x]_{3a}[Ni]_{3b}[O_2]_{6c}$ was adopted to simulate the observed XRD patterns. The refinement strategy was the same as our previous reports [8,9,12,13]. XPS was performed on a Physical Electronics Quantum 2000 ESCA spectrometer. For gaseous product analysis, a MS was connected in the vent side of the tube furnace and operated on a Quadrupole Mass Spectrometer (HPR-20, Hiden Analytical).

Thermal gravimetric analysis (TGA) was carried out using a thermogravimetric analyzer (TA Instruments, model Hi-Res TGA 2950). For the reaction of $LiNiO_2$ with CO_2, fresh $LiNiO_2$ was used as the solid reactant, and CO_2 (99.999%) as the reactant gas. For the reaction of $LiNiO_2$ synthesis, a ball-milled mixture of NiO and Li_2CO_3 was used as the solid reactant, and compressed air as the reactant gas. The TG data under different heating rates, such as 5, 10, 20, 30 and 40 °C min^{-1}, were collected. The reaction activation energy was calculated by the Kissinger method [17,18].

3. Results and discussion

3.1. The reaction between $LiNiO_2$ and CO_2 at room temperature

Figs. 1 and 2 show the XRD patterns of $LiNiO_2$ before and after exposure to CO_2 gas flow for 6 months, together with the simulation patterns of Rietveld refinement. The results of Rietveld refinement are also listed in Table 1. For the sample before reaction with CO_2, the diffraction peaks match well with the indexes of α-$NaFeO_2$ type structure (space group R-3m). There is no other phase that can be found in the XRD pattern. In particular, the peak intensity ratio of $I(0\,0\,3)/I(1\,0\,4)$ is as high as 1.43, suggesting that a well-defined layered structure exists in this sample. However, the Rietveld refinement analysis found that this sample is still non-stoichiometric with a small amount of Ni present in the 3a Li site ($[Li_{1-x}Ni_x]_{3a}[Ni]_{3b}[O_2]_{6c}$, $x = 0.054$). This result is consistent with the ICP-MS result that the atomic ratio of Li/Ni is 0.91. This means that the as-prepared fresh $LiNiO_2$ is still non-stoichiometric with a lack of lithium content although excess lithium was used in the synthesis.

For the $LiNiO_2$ sample after exposure to CO_2 for 6 months, a remarkable change can be seen, that is, a new phase of Li_2CO_3 appears in the XRD pattern. According to the results of Rietveld refinement, the amount of Li_2CO_3 was about 6.96 wt.% in the

Table 1
XRD Rietveld refinement results of (A) fresh $LiNiO_2$ and (B) $LiNiO_2$ after exposure in a pure CO_2 atmosphere at room temperature

Samples	$I(0\,0\,3)/I(1\,0\,4)$	a (Å)	c (Å)	c/a	Ni_{3a} amount	Li_2CO_3 fraction (%)	R_{wp} (%)	R_F (%)
A	1.43	2.87967(3)	14.2001(2)	4.931	0.054(3)	-	10.98	2.51
B	1.16	2.88589(4)	14.2173(3)	4.927	0.131(4)	6.96	12.14	4.65

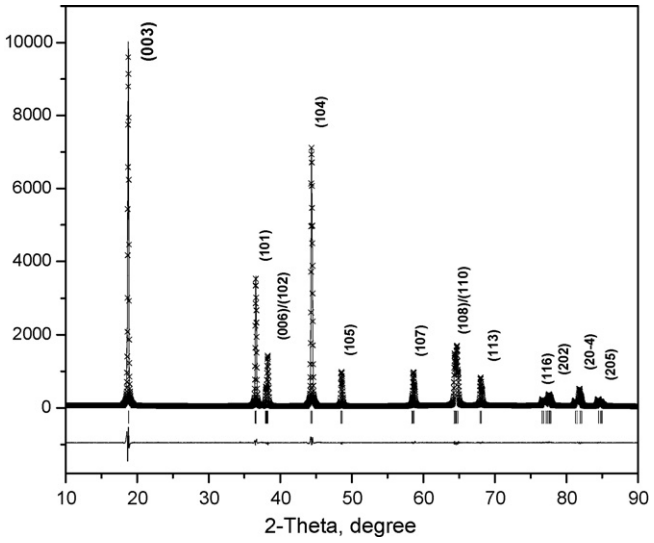

Fig. 1. Measured, calculated and differential XRD patterns of fresh $LiNiO_2$, analyzed by Rietveld refinement. The *x* dots are measured pattern; the solid line is calculated pattern; their differential pattern is shown at the bottom.

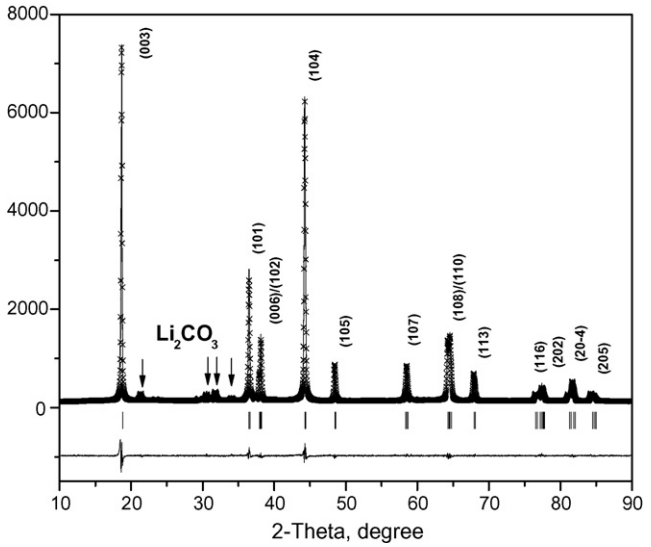

Fig. 2. Measured and calculated differential XRD patterns of $LiNiO_2$ after exposure in a pure CO_2 atmosphere at room temperature, analyzed by Rietveld refinement. The *x* dots are measured pattern; the solid line is calculated pattern; their differential pattern is shown at the bottom.

reacted $LiNiO_2$ sample. Meanwhile, the diffraction peak intensity ratio of $I(0\,0\,3)/I(1\,0\,4)$ was decreased to a value of 1.16. The lattice parameter ratio of *c*/*a* was also decreased from 4.931 to 4.927 although both *a* and *c* were increased after the 6-month exposure to CO_2 gas flow. The structural information indicates that the layered structure ordering of $LiNiO_2$ sample was changed after reaction with CO_2. Rietveld refinement analysis found that the amount of Ni in the 3a Li site was increased to a value of 0.131, suggesting that more nickel ions in the 3b site were transferred into the 3a site during the reaction. In other words, due to the depletion of lithium in forming Li_2CO_3, a part of Li–Ni–O hexagonal crystal units was turned into Ni–O cubic crystal units. Therefore, the reaction between $LiNiO_2$ and CO_2 can not only produce Li_2CO_3, but also change the bulk structure of $LiNiO_2$.

The XPS result, shown in Fig. 3, can give more information about the changes of nickel and oxygen in $LiNiO_2$ after the reaction. As shown, the main Ni 2p peak of the sample before reaction is centred at 856.4 eV, which corresponds to a Ni^{3+} as expected for an ideal $LiNiO_2$. After the reaction with CO_2, the main Ni 2p peak was moved to a value of 854.7 eV, which is characteristic of Ni^{2+}. This means that Ni^{3+} in $LiNiO_2$ was reduced to Ni^{2+} during the reaction with CO_2. On the other hand, the O 1s spectrum was also changed after the reaction. There are two peaks in the O 1s spectrum of un-reacted $LiNiO_2$ sample. The larger one at 528.8 eV can be assigned to the lattice oxygen,

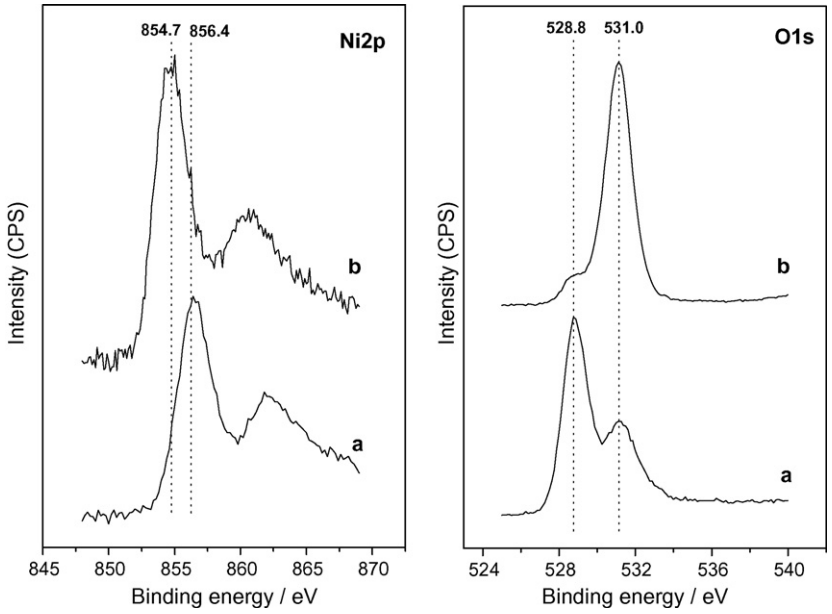

Fig. 3. Ni 2p and O 1s XPS patterns of $LiNiO_2$ (a) before and (b) after exposure in a pure CO_2 atmosphere at room temperature.

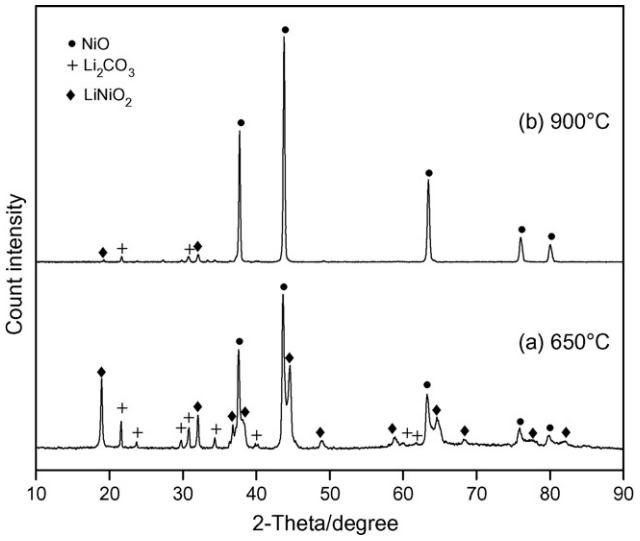

Fig. 4. XRD patterns of $LiNiO_2$ reacted with CO_2 in a pure CO_2 atmosphere at 650 and 900 °C, respectively.

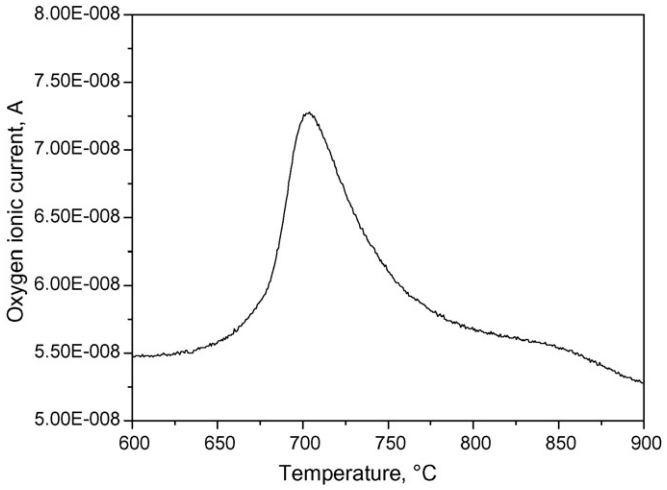

Fig. 5. Mass spectroscopy signal of oxygen as the product of $LiNiO_2$ reacted with CO_2 in a pure CO_2 atmosphere.

while the smaller one at 531.0 eV to adsorbed surface oxygen species or trace amount of CO_3^{2-} impurity. After the reaction, the peak at 531.0 eV became the main peak while the peak at 528.8 eV was reduced dramatically. This indicates that the surface of $LiNiO_2$ was largely covered by the formed Li_2CO_3 after the 6-month exposure in CO_2. Meanwhile, this result also suggests that the lattice oxygen in the bulk material might participate in the formation of Li_2CO_3 because there was no other oxygen source to assist CO_2 to complete the reaction.

In summary, the analysis of the reaction between $LiNiO_2$ and CO_2 in a pure CO_2 atmosphere at room temperature confirms that Li_2CO_3 is the product of this reaction, that the bulk Ni^{3+} can be reduced to Ni^{2+} during the reaction, and that the bulk lattice oxygen can participate in this reaction. However, it is believed that the analysis of the reaction at high temperature can give more evidence about the reaction mechanism, which will be presented in the following section.

3.2. The reaction between $LiNiO_2$ and CO_2 at high temperature

Fig. 4 shows the XRD patterns of the $LiNiO_2$ sample after reaction with CO_2 at 650 and 900 °C, respectively. For the sample reacted at 650 °C, three phases, i.e. $LiNiO_2$, Li_2CO_3, and NiO, can be found. This provides direct evidence that Li_2CO_3 and NiO are the solid products of this reaction. The production of NiO at high temperature is consistent with the reduction of Ni^{3+} to Ni^{2+} in the room temperature reaction. When the reaction temperature increases to 900 °C, $LiNiO_2$ almost disappeared and NiO became the main phase, as seen in the XRD pattern. In the mean time, Li_2CO_3 also nearly disappeared, which is possibly because Li_2CO_3 could be completely melted and penetrated into the ceramic combustion boat at such a high temperature. In order to detect the possible gaseous product generated by such a high temperature reaction, a Quadrupole Mass Spectrometer was connected to the vent side of the tube furnace during the heating process. Fig. 5 shows the oxygen concentration (expressed as ionic current) detected in the vent gas as a function of heating temperature. The oxygen signal remains relatively stable before 625 °C. When the temperature is greater than 625 °C, a dramatic increase in oxygen concentration can be observed. After 705 °C, further increasing temperature can result in a wide peak. This peak signal gives a clear indication that oxygen gas is also one of the products of the reaction between $LiNiO_2$ and CO_2. This information obtained at high temperatures is very useful in clarifying the reaction mechanism.

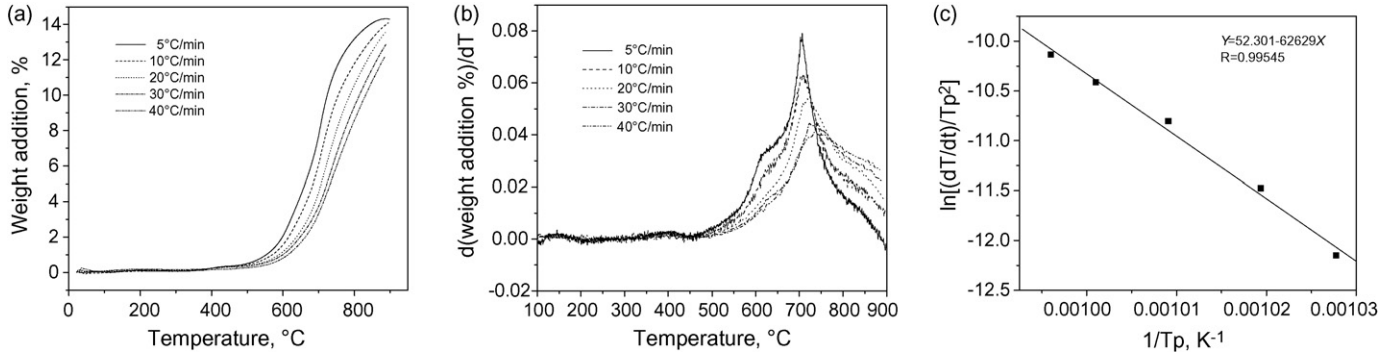

Fig. 6. (a) TGA curves of $LiNiO_2$ in CO_2 atmosphere at different heating rates; (b) The differential curves corresponding to (a); (c) The plot of $\ln[(dT/dt)/T_p^2]$ vs. $1/T_p$, from which the activation energy can be calculated.

Thus, based on the observations both at low and high temperatures, the reaction mechanism between $LiNiO_2$ and CO_2 can be deduced as the following equation:

$$LiNiO_2 + 0.5CO_2 \leftrightarrow NiO + 0.5Li_2CO_3 + 0.25O_2 \quad (3)$$

The TGA curve and its differential curve under a slow heating rate of 5 °C min^{-1}, as shown in Fig. 6 (a) and (b), can further confirm this reaction equation. In reaction (3), the produced solid sum weight of $NiO + 0.5Li_2CO_3$ is heavier than that of the reactant $LiNiO_2$. Therefore, the reaction between $LiNiO_2$ and CO_2 is a weight addition reaction if the weights of gaseous reactant ($0.5CO_2$) and product ($0.25O_2$) are not counted. As shown in Fig. 6, the weight addition begins at around 500 °C and reaches a plateau at 900 °C. The maximum weight addition is 14.1%, which is very close to the value of 14.3% theoretically expected from Eq. (3). The differential curve shows two peaks. The first shoulder peak around 600 °C indicates that the reaction was impeded when the formed Li_2CO_3 largely covered the surface of $LiNiO_2$. After Li_2CO_3 melted at temperatures higher than 650 °C, the reaction resumed and produced a sharp peak centred at 703 °C.

In fact, Eq. (3) should be a reversible reaction depending on the concentrations (partial pressure of CO_2 and O_2) of the reactants and the temperature. For example, the forward direction of this reaction is the surface Li_2CO_3 formation (NiO, Li_2CO_3 and O_2 production) and the back reaction is the formation of $LiNiO_2$ and CO_2 through the reaction of NiO, Li_2CO_3 and O_2 ($LiNiO_2$ synthesis process). Obviously, the competition of the two reactions is significant to the synthesis and storage property of $LiNiO_2$ material. A kinetics analysis of the two reactions will be discussed in the following section.

3.3. Reaction activation energy and kinetics analysis

The Kissinger method [17,18] was used for the evaluation of the reaction activation energy based on TGA measurements:

$$-\ln(\beta T_p^2) = -\ln\left(\frac{AR}{E_a}\right) + \left(\frac{1}{T}\right)\left(\frac{E_a}{R}\right)$$

where E_a is the reaction activation energy, T_p the reaction peak temperature, β the heating rate (dT/dt), R the gas constant and A is the frequency factor. The slope of $\ln(\beta/T_p^2) \sim 1/T_p$ plot allows one to evaluate the activation energy.

For the reaction between $LiNiO_2$ and CO_2, TGA curves at five heating rates, such as 5, 10, 20, 30 and 40 °C min^{-1}, were collected, as shown in Fig. 6(a). Corresponding to each heating rate, the peak temperatures were determined to be 700, 708, 718, 726 and 731 °C, respectively, by the differential TGA curves as shown in Fig. 6(b). The reaction activation energy was then calculated to be 521 kJ mol^{-1} from the plot of $\ln(\beta/T_p^2) \sim 1/T_p$ in Fig. 6(c). Using the same procedure, the TGA curves for the back reaction from NiO, Li_2CO_3 and O_2 to $LiNiO_2$ and CO_2 can also be obtained, as shown in Fig. 7(a). The peak temperatures are 702, 710, 716, 721 and 725 °C, respectively, as shown in Fig. 7(b). The activation energy of the synthesis reaction was calculated to be 733 kJ mol^{-1} by the plot of $\ln(\beta/T_p^2) \sim 1/T_p$ in Fig. 7(c). Note that Chang et al. [18] also used the Kissinger method to evaluate the activation energy of the $LiNiO_2$ synthesis through the xerogel precursor. They obtained the activation energy of 98 kJ mol^{-1}, which is much different from our result. This difference may be caused by the different reaction mechanisms. In Chang et al.'s work, the used xerogel process in a wet environment could be a one-step reaction while the direct solid-state process in this work may be a two-step reaction [18]. The reaction activation energy is actually a kinetic parameter, the value of which is strongly dependent on the reaction mechanism.

The overall Gibbs energy (ΔE) of Eq. (3) can be calculated as:

$$\Delta E = E_a^f - E_a^b = 521\,\text{kJ mol}^{-1} - 733\,\text{kJ mol}^{-1} = -212\,\text{kJ mol}^{-1}$$

where E_a^f is the reaction activation energy of the forward direction, and E_a^b is that of the back reaction. Apparently, the reaction (3) is a thermodynamically favoured reaction either at room temperature or high temperature. This may be one of the main reasons why Li_2CO_3 can be easily formed on the surface of $LiNiO_2$ during the storage in air. As per the Arrhenius equation, we can obtain the reaction rate equations as follows:

$$v_f = A_f \exp\left(\frac{-E_a^f}{RT}\right) P_{CO_2}^x$$

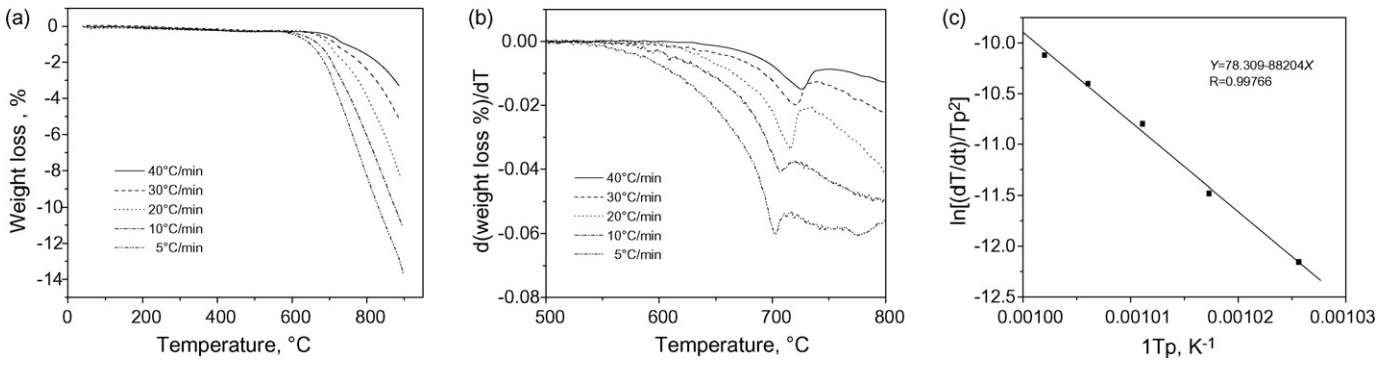

Fig. 7. (a) TGA curves of the reaction of NiO with Li_2CO_3 in air at different heating rates; (b) The differential curves corresponding to (a); (c) The plot of $\ln[(dT/dt)/T_p^2]$ vs. $1/T_p$, from which the activation energy can be calculated.

$$v_b = A_b \exp\left(\frac{-E_a^b}{RT}\right) P_{O_2}^y$$

$$\frac{v_f}{v_b} = A \exp\left(\frac{-\Delta E}{RT}\right) \frac{P_{CO_2}^x}{P_{O_2}^y}$$

where v_f is the rate of the forward reaction of $LiNiO_2$ with CO_2, v_b the rate of the back reaction ($LiNiO_2$ synthesis reaction), P_{CO_2} the partial pressure of CO_2, P_{O_2} the partial pressure of O_2, x and y are the unknown reaction orders for CO_2 and O_2, respectively. From the reaction rate equations, it can be found that the reaction of $LiNiO_2$ with CO_2 is faster than the reaction of $LiNiO_2$ synthesis from an energy point of view. In the synthesis of $LiNiO_2$ through the precursors of NiO, Li_2CO_3 and O_2, the overall reaction rate depends on the temperature and the gas partial pressures. Higher temperature (below the decomposition temperature of $LiNiO_2$), lower CO_2 partial pressure and higher O_2 partial pressure facilitate the synthesis of $LiNiO_2$.

4. Conclusions

The mechanism and kinetics of the reaction between $LiNiO_2$ and CO_2 were investigated in a pure CO_2 atmosphere. It was found that during the reaction at room temperature Li_2CO_3 is one of the reaction products, that the bulk Ni^{3+} is reduced to Ni^{2+} to form NiO, and that the bulk lattice oxygen also participates in this reaction. The studies at high temperature confirmed that the products of this reaction are Li_2CO_3, NiO, and O_2.

The reaction between $LiNiO_2$ and CO_2 is a reversible reaction depending on the concentrations of the reactants and the temperature. The forward direction of this reaction is the surface Li_2CO_3 formation (NiO, Li_2CO_3 and O_2 production) and the back reaction is the formation of $LiNiO_2$ and CO_2 through the reaction of NiO, Li_2CO_3 and O_2 ($LiNiO_2$ synthesis process). Kinetics analysis showed that the forward reaction between $LiNiO_2$ and CO_2 is thermodynamically favourable, and the reaction rate is faster than the reverse synthesis reaction from the energy view of point. These results are helpful in understanding the poor storage property of $LiNiO_2$ and the low synthesis reproducibility of $LiNiO_2$ cathode material for lithium ion batteries.

Acknowledgements

This work was financially supported by NRC Institute for Fuel Cell Innovation and Xiamen University. Mr. Eric Fuller is highly appreciated for his assistance in the mass spectroscopy measurement. Ms. Marianne Rodgers is highly appreciated for her English proofreading.

References

[1] J.M. Tarascon, M. Armand, Nature 414 (2001) 361.
[2] P. Kakyani, N. Kalaiselvi, Sci. Technol. Adv. Mater. 6 (2005) 689.
[3] A. Ueda, T. Ohzuku, J. Electrochem. Soc. 141 (1994) 2010.
[4] Y. Gao, M.V. Yakovleva, W.B. Ebner, Electrochem. Solid-State Lett. 1 (1998) 117.
[5] K. Matsumoto, R. Kuzuo, K. Takeya, A. Yamanaka, J. Power Sources 81/82 (1999) 558.
[6] D.P. Abraham, R.D. Twesten, M. Balasubramanian, I. Petrov, J. MacBreen, K. Amine, Electrochem. Commun. 4 (2002) 620.
[7] A.M. Andersson, D.P. Abraham, R. Haasch, S. MacLaren, J. Liu, K. Amine, J. Electrochem. Soc. 149 (2002) A1358.
[8] H.S. Liu, J. Li, Z.R. Zhang, Z.L. Gong, Y. Yang, J. Solid State Electrochem. 7 (2003) 456.
[9] H.S. Liu, J. Li, Z.R. Zhang, Z.L. Gong, Y. Yang, Electrochim. Acta 49 (2004) 1151.
[10] G.V. Zhuang, G. Chen, J. Shim, X. Song, P.N. Ross, T.J. Richardson, J. Power Sources 134 (2004) 293.
[11] S.W. Song, G.V. Zhuang, R.N. Ross, J. Electrochem. Soc. 151 (2004) A1167.
[12] H.S. Liu, Z.R. Zhang, Z.L. Gong, Y. Yang, Electrochem. Solid-State Lett. 7 (2004) A190.
[13] H.S. Liu, Y. Yang, J.J. Zhang, J. Power Sources 162 (2007) 644.
[14] J. Kim, Y. Hong, K.S. Ryu, M.G. Kim, J. Cho, Electrochem. Solid-State Lett. 9 (2006) A19.
[15] K. Shizuka, C. Kiyohara, L. Shima, Y. Takeda, J. Power Sources 166 (2007) 233.
[16] A.C. Larson, R.B. Von Dreele, LANSCE, MS-H805, Los Alamos National Laboratory, Los Alamos, NM.
[17] D. Chen, X. Gao, D. Dollimore, Thermochim. Acta 215 (1993) 109.
[18] C.C. Chang, J.Y. Kim, P.N. Kumta, J. Electrochem. Soc. 149 (2002) A331.